Study of the lattice dynamics of hexagonal close-packed ^{3}He and ^{4}He using inelastic x-ray scattering

1999 J. Phys.: Condens. Matter 11 3501

(http://iopscience.iop.org/0953-8984/11/17/308)

J. Phys.: Condens. Matter **11** (1999) 3501–3511. Printed in the UK PII: S0953-8984(99)01359-4

Study of the lattice dynamics of hexagonal close-packed ^{3}He and ^{4}He using inelastic x-ray scattering

C Seyfert†, R O Simmons‡, H Sinn†, D A Arms‡ and E Burkel†

† FB Physik, Universität Rostock, 18051 Rostock, Germany
‡ Department of Physics, University of Illinois, Urbana-Champaign, IL 61801, USA

Received 28 January 1999, in final form 19 March 1999

Abstract. We present the first measurement of the coherent dynamic structure factor $S(\boldsymbol{Q}, \omega)$ of solid ^{3}He. At a density of 13.25(10) cm^3 mol^{-1}, we observed longitudinal phonons, using high-resolution inelastic x-ray scattering at momentum transfers $6\,\mathrm{nm}^{-1} < |\boldsymbol{Q}| < 23\,\mathrm{nm}^{-1}$. Their dispersion relation was determined along the c-axis in single crystals of hcp ^{3}He, and the spectra were described with a single-phonon model. For comparison, hcp ^{4}He at the same density was studied with the same technique. The comparison, including all available ^{4}He data from neutron scattering experiments, results in a phonon frequency ratio ω_3/ω_4 of 1.11(5). Special attention is given to the scattering contribution due to multi-phonon excitations.

1. Introduction

Solid and liquid helium are ideal systems on which to base a study of the influence of quantum effects on condensed matter. The well known interatomic potential and the availability of two isotopes with different quantum statistics and a large relative mass difference has made it a model system for theoretical work. In addition, a wide range of densities and temperatures are experimentally accessible, allowing theories to be tested stringently. In particular, the dynamics of helium has been of continuous interest.

The dynamics of liquid and solid ^{4}He and of liquid ^{3}He has been probed extensively by means of inelastic neutron scattering [1]. However, there is a striking lack of experimental data on the inelastic excitation spectra of solid ^{3}He [2]. This is mainly due to the high absorption cross section of ^{3}He for thermal neutrons, a major complication for the neutron scattering experiments on liquid ^{3}He [3]. In addition, to study the lattice dynamics of the solid, it is necessary to work with single crystals of appropriate size. These have to be grown in a suitable high-pressure environment, since helium only solidifies under externally applied pressure, even at the lowest temperatures.

Theoretical study of the lattice dynamics in the highly anharmonic solid has also concentrated on ^{4}He [1, 2]. Phonon frequencies and interesting multi-phonon phenomena in ^{4}He have been qualitatively interpreted using self-consistent phonon (SCP) theories. However, the agreement between the calculated and measured phonon energies for ^{4}He has been typically $\pm 20\%$, which is larger than the raw mass ratio $\sqrt{4/3}$. Due to its lower mass and correspondingly larger vibrational amplitudes, ^{3}He probes more of the anharmonic potential than ^{4}He does. Still, very little analysis [2] has been devoted to ^{3}He models due to the absence of experimental data.

0953-8984/99/173501+11$19.50

We chose the technique of very-high-resolution inelastic x-ray scattering to study the lattice dynamics in solids of both isotopes, ^{3}He and ^{4}He. The feasibility of using inelastic x-ray scattering to study condensed ^{4}He has been demonstrated at the spectrometer INELAX at HASYLAB in Hamburg [4]. The third-generation synchrotron ESRF in Grenoble allowed studies to be carried out with much higher accuracy. Preliminary data on the phonon dispersion relation for hcp ^{3}He and ^{4}He have already been published elsewhere [5, 6].

2. Experimental procedure

The experiments reported here were carried out at ID16, ESRF. Basically, ID16 is a triple-axis spectrometer with an additional heat load monochromator, situated at an undulator source of the ESRF. To achieve a relative energy resolution better than 5×10^{-7}, high-order reflections from perfect silicon crystals in backscattering geometry are used. The monochromator and analyser angles are kept fixed; the energy transfer ω is changed by thermal variation of the lattice parameter of the monochromator crystal. The momentum transfer $\boldsymbol{Q}$ is selected by choosing the appropriate scattering angle in the vertical scattering plane. In contrast to the energy resolution function for inelastic neutron scattering, the resolution function in an elastic x-ray scattering experiment is constant in $(\boldsymbol{Q}, \omega)$ space. Details of the backscattering technique and instrumental details can be found in references [7, 8].

Three sets of experiments were performed with different energy resolutions: using Si(7, 7, 7) reflections at 13.8 keV, the energy resolution for the experiment on ^{4}He was 8.6 meV (FWHM) while a value of 8.2 meV was determined for the first ^{3}He measurements. The follow-up experiment on ^{3}He was done with a resolution of 5.9 meV at 17.8 keV using Si(9, 9, 9) reflections for the monochromator and analyser. Energy scans at constant momentum transfer and fixed final energy were performed. The tuning of the incident energy was done by varying the temperature of the monochromator every 30 seconds in steps of 0.01 K. This corresponds to energy steps of 0.35 meV at 13.8 keV and 0.45 meV at 17.8 keV. A well focused beam with a cross section of 300×500 μm^2 allowed us to work with small crystals. Also, at the x-ray energies used, the absorption in the helium sample is negligible.

Single crystals of hcp ^{3}He and ^{4}He were grown *in situ* within a polycrystalline beryllium pressure cell [9] of 1.2 mm inner diameter. The cell was mounted inside a Leybold RGD 5/100 T closed-cycle refrigerator with a base temperature of 6.5 K. The sample cell was pressurized with helium gas via a capillary from the external pressure-generating system [10]. At an almost constant pressure of 90 MPa (70 MPa in the case of ^{4}He), the cell was slowly cooled down to below the freezing temperature. Due to a controlled temperature gradient along the cell, single-crystal growth was enhanced. However, crystals had to be oriented and characterized individually, using their Bragg reflections. Suitable single crystals were then kept at temperatures between 7.7 and 9.6 K, well below their freezing points.

For the hcp ^{3}He crystals, the measured c-axis lattice parameters were 5.124(20) Å and 5.144(15) Å, corresponding to molar volumes of 13.2(1) cm^3 and 13.3(1) cm^3, respectively. This is consistent with the melting points determined, 12.0(3) K and 11.85(20) K, and the equation of state of ^{3}He [11]. In the case of hcp ^{4}He, the values were 5.124(30) Å and 11.0(3) K, respectively. The mosaic spread of the crystals was typically about 0.05°.

3. Data analysis

The scattered intensity was normalized for each scan with respect to a monitor counter measuring the actual flux incident on the sample. Inelastic x-ray spectra, $I(\boldsymbol{Q}, \omega)$, are shown

in figure 1 for selected values of the momentum transfers $\boldsymbol{Q}$ along the [001] direction. The energy transfer from the photon to the sample is denoted by ω. The spectra are characterized by two peaks, an elastic line and the helium phonon. Note that only the Stokes line ($\omega > 0$) is observed at low temperatures, since the thermal occupation factor $\langle n \rangle$ for phonon annihilation is strongly suppressed. The dispersion of the phonon energy with momentum transfer is already evident in the raw data.

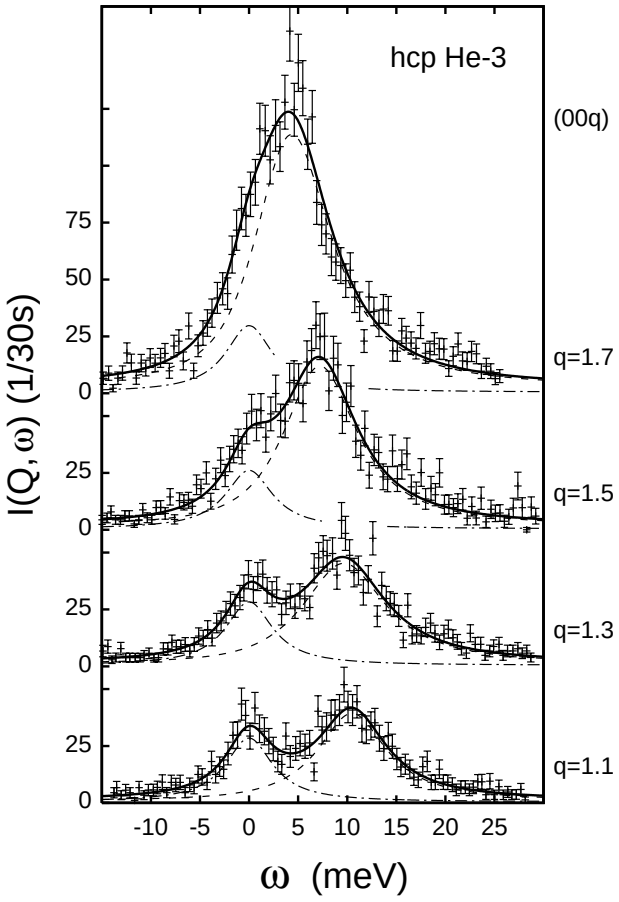

Figure 1. Inelastic x-ray spectra of hcp ^{3}He for selected momentum transfers $Q = q\,2\pi/c$ along the [001] direction. The solid curves are fits to the data, according to equations (1) and (2). The dash–dotted curves show the elastic contributions of the sample environment at $\omega = 0$; their shapes are determined by the resolution function. The dashed curves represent the phonon, described by a damped harmonic oscillator convoluted with the resolution function.

The measured intensity $I(\boldsymbol{Q}, \omega)$ is given by the convolution of the dynamic structure factor $S(\boldsymbol{Q}, \omega)$ and the resolution function $R(\omega)$ which is independent of the momentum transfer:

$$I(\boldsymbol{Q}, \omega) \propto \int_{-\infty}^{+\infty} (a\delta(\omega') + S(\boldsymbol{Q}, \omega'))R(\omega - \omega')\,\mathrm{d}\omega'. \tag{1}$$

Here, the delta function denotes elastic scattering. It can be ascribed mostly to the scattering of the polycrystalline beryllium sample cell, as identified by empty-cell scans. Its intensity depends on the actual orientation and alignment of the polycrystalline sample cell. Therefore,

the amplitude a is treated as a fit parameter. The elastic scattering is used to calibrate the zero point of the energy-transfer scale of the individual scans. This is necessary since drifts of this energy zero of up to 2 meV have been observed. Temperature drifts of the analyser crystal are the most likely reason for this behaviour, although its temperature is constantly monitored and controlled. However, if the sensor temperature lags behind the actual temperature of the crystal, this will lead to a systematic drift. Except for these shifts, scans taken at the same momentum transfer are reproducible within statistical accuracy. The energy calibration is described in detail in [10]. Its overall uncertainty is estimated to be less than 3%. No significant inelastic contribution from the sample cell or sample environment has been observed in the energy-transfer range of interest. The beryllium phonons are only visible at much higher energy transfer.

In the energy- and momentum-transfer ranges for which the experiment was performed, the expected $S(\boldsymbol{Q}, \omega)$ of solid helium is purely coherent. For the analysis, we describe it by a damped harmonic oscillator (DHO), according to a discussion given by Fåk and Dorner [12]:

$$S_{\mathrm{fit}}(\boldsymbol{Q}, \omega) = \frac{Z_q(\boldsymbol{Q})}{1 - \mathrm{e}^{-\hbar\omega/k_B T}} \frac{\omega\omega_q\Gamma_q}{(\omega^2 - (\omega_q^2 + \Gamma_q^2))^2 + 4\omega^2\Gamma_q^2}. \tag{2}$$

This function was convoluted with the Lorentzian resolution function to fit the observed spectra. No background correction was necessary. $Z_q(\boldsymbol{Q})$ denotes the phonon structure factor. The term $(1 - \exp(-\hbar\omega/k_B T))^{-1}$ takes care of the detailed balance between the energy-loss and energy-gain processes. The lifetime broadening Γ_q is vanishing in the harmonic approximation. However, anharmonicity leads to finite lifetimes and $\Gamma_q > 0$. Fåk and Dorner suggest using

$$\Omega_q = \sqrt{\omega_q^2 + \Gamma_q^2}$$

as the physically relevant phonon energy, rather than ω_q which corresponds to the observed peak position. However, we prefer to use ω_q as the phonon frequency, in order to facilitate comparison with the experimental data on ^{4}He available from inelastic neutron scattering experiments.

Obviously, the description of the inelastic spectra with a DHO model ignores any contributions from multi-phonon excitations. However, the experimental data could be described by this model in a consistent way. Bootstrap Monte Carlo simulations [13] were applied to check the stability of the fit and to estimate the accuracy of the fit parameters. The influence of higher-order contributions will be discussed in section 5.3.

4. Results

4.1. The dispersion relation of hcp ^{4}He along [001]

The dispersion relation of longitudinal Δ_2 and Δ_1 phonons in hcp ^{4}He was determined in the second and third Brillouin zones, respectively. This corresponds to a momentum-transfer range of $12.5\ \mathrm{nm}^{-1} < |\boldsymbol{Q}| < 23.5\ \mathrm{nm}^{-1}$. The momentum resolution was $0.7\ \mathrm{nm}^{-1}$.

To compare the measured phonon dispersion relation with the data available from neutron scattering experiments, it is necessary to scale the phonon frequencies to a common density. This was done using the temperature-independent Grüneisen parameter γ_0, determined by Ahlers [14] as $\gamma_0 = 1.02 + 0.083V$, with V the molar volume in cm^3. Thus, the phonon frequencies scale as

$$\ln(\omega_1/\omega_2) = 0.083(V_1 - V_2) + 1.02\ln(V_1/V_2). \tag{3}$$

All available neutron data [15–18] on longitudinal phonons in the c-direction of hcp ^{4}He are shown together with the inelastic x-ray scattering data in figure 2, scaled accordingly. The agreement of the Δ_1 branch is excellent, considering the big molar volume range from 21.1 cm^3 to 9.41 cm^3. However, there is substantial scatter for the high-lying Δ_2 branch. This scatter is not volume systematic, but might be caused by the different procedures used to extract the single-phonon contribution from the measured data.

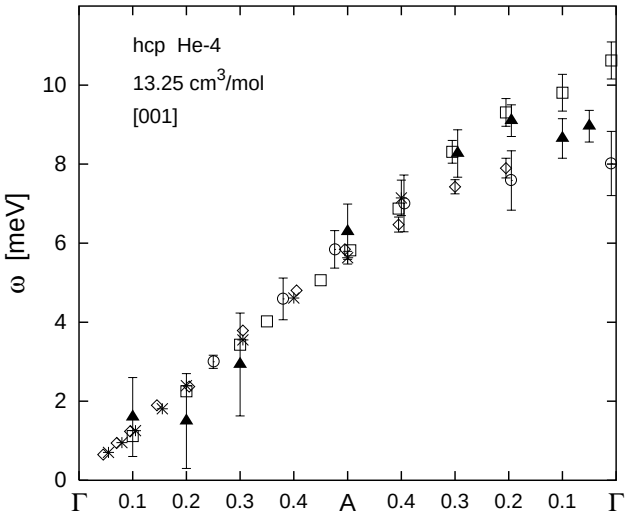

Figure 2. Comparison of all available data on the longitudinal phonon dispersion relation along [001] in hcp ^{4}He displayed in the reduced-zone scheme. The data are scaled to a molar volume of 13.25 cm^3 according to a formula given in [14]. Neutron measurements: circles: 21.1 cm^3 [15,16]; boxes: 16.0 cm^3 [17]; stars: 11.6 cm^3; and diamonds: 9.4 cm^3 [18]. The filled triangles show the 13.3 cm^3 x-ray data.

4.2. Longitudinal phonons in hcp ^{3}He

For the first time, a dispersion relation for solid ^{3}He was determined. For longitudinal Δ phonons in hcp ^{3}He, it was mapped out between (0, 0, 0.5) at the zone boundary between the first and second Brillouin zones and (0, 0, 1.9) close to the zone centre of the third Brillouin zone. This corresponds to a momentum-transfer range of 6 nm^{-1} $< |\boldsymbol{Q}| <$ 23 nm^{-1}.

The phonon dispersion relation determined and the corresponding full width at half-maximum $2\Gamma_q$ are shown in figure 3. The stated errors are the uncertainties after averaging over repeated scans performed during two beam-times. A sound velocity of 1710(60) m s^{-1} was deduced from the slope of the dispersion relation of the Δ_1 branch.

The Δ_2 phonon frequencies show a deviation from the expected symmetry about the zone centre Γ: $\omega(q)$ is lower below (0, 0, 1) than above. Interference between one-phonon and multi-phonon processes, as discussed by Glyde [1], is a likely explanation for this behaviour.

More prominent is the asymmetry around (0, 0, 1) in the observed width parameter Γ_q. Below $q = 1.0$, we did not observe any substantial line broadening; the phonons are well defined sharp excitations. However, at higher momentum transfers, the peak widths increase and reach their maximum at $q = 1.6$. There, the ratio ω_q/Γ_q is less than two. Closer to the Bragg reflection (0, 0, 2), the width is decreasing again. This behaviour is a strong indication that the measured spectra at higher momentum transfers are influenced by additional broader

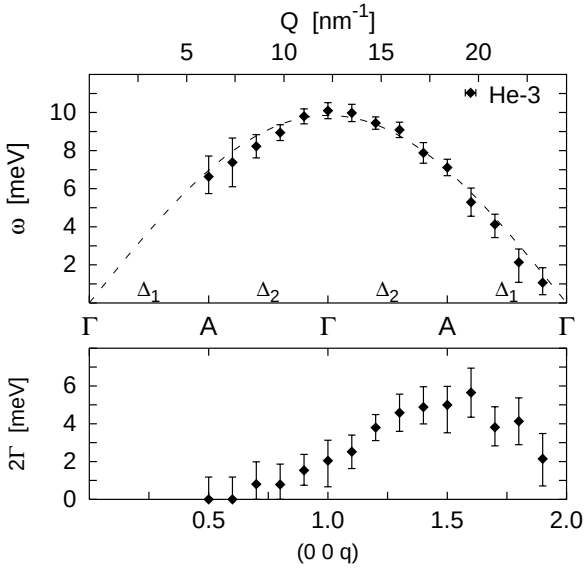

Figure 3. Top: the phonon dispersion relation for longitudinal phonons in hcp ^{3}He along the [001] direction in the extended-zone scheme. The dashed curve is a one-parameter fit to a monatomic linear chain model. Bottom: the corresponding observed phonon linewidth 2Γ (FWHM).

contributions from multi-phonon processes, as will be discussed later.

The inelastic x-ray scattering experiments on hcp ^{4}He at the same density showed similar behaviour. However, the uncertainty in determining the intrinsic phonon linewidth in those experiments is even higher due to a broader resolution function. Reese *et al* [17] report a different q-dependent line broadening in hcp ^{4}He at a molar volume of 16.0 cm^3. For the longitudinal branch along Γ–A–Γ, they measured insignificant line broadening for the Δ_1 branch, but a strong increase in width for Δ_2 approaching the zone centre Γ. The observed maximum width is about 4 meV at a phonon energy of 6.5 meV. Unfortunately, Reese *et al* did not compare linewidths of symmetrically equivalent phonons in different Brillouin zones.

We also measured the longitudinal dynamic structure factor along the [100] direction in

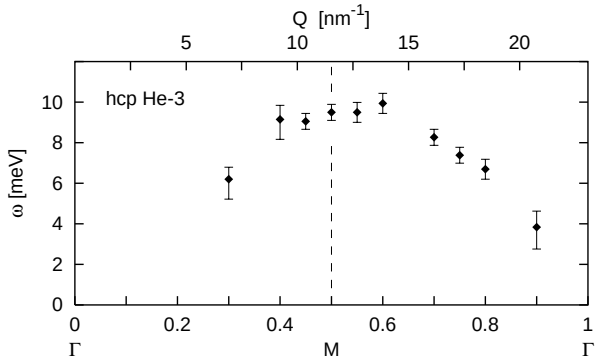

Figure 4. The dispersion of the observed longitudinal excitation in hcp ^{3}He along the [100] direction. Plotted is the maximum of $S_{\rm fit}(\boldsymbol{Q}, \omega)$.

hcp ^{3}He. However, we were not able to separate the Σ_1(LA) and the Σ_1(LO) branches with the energy resolution achieved. In the experimental spectra, only one broad component is observable. Therefore, in figure 4 we show the maximum of the inelastic contribution. As the upper limit for the difference between the phonon frequencies of Σ_1(LA) and Σ_2(LO), we estimated a value of 2.5 meV.

4.3. Intensity and the Debye–Waller factor

For completeness, we want to mention the observed intensities, though the experiments were not optimized for intensity measurements. Therefore, only the data from the last beam-time for hcp ^{3}He will be discussed. Figure 5 shows the Debye–Waller factor $d^2_{\mathrm{DW}}(\boldsymbol{Q})$. In first-order approximation, the static structure factor $S(\boldsymbol{Q})$ for the longitudinal branch of hcp ^{3}He in the [001] direction is given by

$$S(\boldsymbol{Q}) \propto d^2_{\mathrm{DW}}(\boldsymbol{Q})Q^2/\omega_p. \tag{4}$$

$S(\boldsymbol{Q})$ was obtained by integration of $S_{\mathrm{fit}}(\boldsymbol{Q}, \omega)$ (equation (2)), the fitted inelastic intensities. It was normalized using $d^2_{\mathrm{DW}}(Q = 0) = 1$. From these data, a mean square deviation of the ^{3}He atoms from their lattice site $\langle u^2 \rangle$ of 0.142(17) Å^2 results. This is in excellent agreement with the value 0.140 Å^2 extrapolated from the Debye–Waller factor measurements of Arms [19].

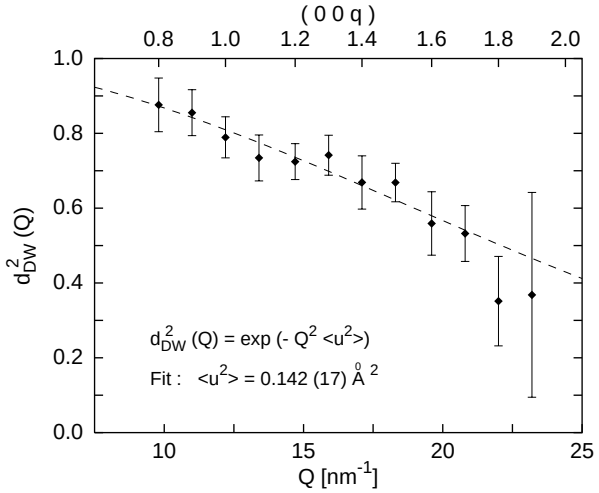

Figure 5. The Debye–Waller factor determined from a plot of $S(\boldsymbol{Q})\omega_p/Q^2$.

5. Discussion

5.1. Comparison with calculations

In contrast to that of the cubic phases, the lattice dynamics of the hexagonal hcp phase of helium has attracted only little theoretical interest. Gillis *et al* [20] studied the low-density regime 21–16 cm^3 mol^{-1} of hcp ^{4}He, using a SCP model. However, the—according to the authors—unsatisfactory density dependence of their theory prevents a meaningful extrapolation of the calculated phonon frequencies to higher densities.

The only other relevant calculation was carried out by Morley and Kliewer [21]. They performed a self-consistent harmonic (SCH) calculation for both isotopes of hcp helium

at molar volumes between 10 and 16 cm^3. At 13.25 cm^3 mol^{-1}, their computed phonon frequencies are about 25% higher than the observed frequencies for ^{3}He and ^{4}He. As was pointed out by Chell *et al* [22], this discrepancy is probably caused by the neglect of the cubic anharmonic term in the calculation.

Both studies concentrate on the phonon dispersion relation only and do not consider lineshapes, multi-phonon excitations and related topics. Thus, the direct comparison of observed lineshapes with calculations is not possible at the moment. Some qualitative discussion based on calculations for cubic ^{4}He is given in section 5.3.

5.2. The ^{3}He-to-^{4}He phonon frequency ratio

A plot showing ratios of the frequencies for ^{3}He and ^{4}He for different reduced q-values is shown in figure 6. Comparison with neutron data was performed for the Δ_1 branch and at $q_{\mathrm{red}} = 0.4$ for the Δ_2 branch only, due to the scatter of the neutron data for the Δ_2 branch closer to the zone centre (see figure 2). On the other hand, the low-lying ^{4}He data measured by means of x-rays have a high uncertainty and are therefore discarded for the ratio determination. There appears to be a slight systematic difference between the ratios for the Δ_1 branch and the Δ_2 branch. This suggests a difference between the shapes of the dispersion relations for ^{3}He and ^{4}He. However, the q-resolved data available from inelastic neutron and x-ray scattering investigations are not conclusive there.

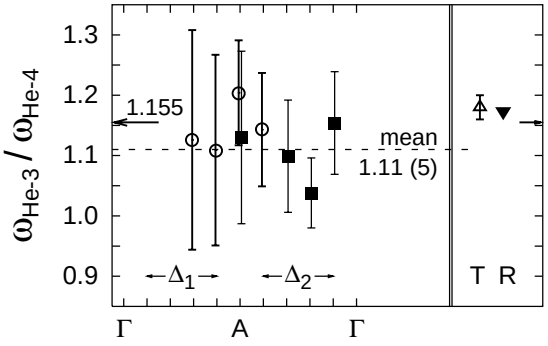

Figure 6. The ratio of the phonon frequencies plotted for different reduced wave vectors q_{red}. Circles indicate ratios with ^{4}He frequencies taken from neutron scattering, while ratios marked with boxes are determined from inelastic x-ray scattering only. The error bars give the combined uncertainties of the ^{3}He and ^{4}He phonon frequency measurements. The arrows at $\sqrt{4/3} = 1.155$ indicate the classical ratio expected from the mass difference alone. The weighted average is 1.11(5). For comparison, the triangles give values obtained by Debye temperature measurements (T, from [23]) and from Raman scattering (R, from [24]).

Ignoring any possible q-dependence, the weighted mean frequency ratio of $\omega_{^3\mathrm{He}}$ to $\omega_{^4\mathrm{He}}$ is 1.11(5). This has to be compared with the ratio expected for a classical harmonic crystal, i.e. the square root of the inverse masses, $\sqrt{4/3} = 1.155$. On the other hand, the SCH calculation for this molar volume [21] yielded the value 1.25. Experimentally, a value of 1.18 was obtained by Sample and Swenson [23] from the low-temperature limit of the Debye characteristic temperatures Θ_0 of ^{3}He and ^{4}He. These were determined by heat capacity measurements over a range of molar volumes in the hcp phases of both isotopes and therefore weight the phonon frequency distribution $g(\omega)$ by a factor ω^{-3}. An additional value is reported by Slusher and Surko [24] for the ratio of transverse phonon frequencies in hcp ^{3}He and ^{4}He at $q = 0$. They determined a value of 1.17(1) by means of Raman scattering from a low-frequency zone-centre

optical phonon in hcp helium at densities between 18 and 20 cm^3 mol^{-1}. The Δ branches reported in this paper are not Raman active.

5.3. Lineshape and multi-phonon contributions

The dynamic structure factor $S(\boldsymbol{Q}, \omega)$ for anharmonic solids is usually expanded [1] as

$$S(\boldsymbol{Q}, \omega) = S_1(\boldsymbol{Q}, \omega) + S_{12}(\boldsymbol{Q}, \omega) + S_2(\boldsymbol{Q}, \omega) + \cdots. \tag{5}$$

Here, $S_1(\boldsymbol{Q}, \omega)$ denotes the pure one-phonon contribution, $S_2(\boldsymbol{Q}, \omega)$ denotes processes involving two phonons, while $S_{12}(\boldsymbol{Q}, \omega)$ is the term describing the interference between these two contributions. Only at low momentum transfer is $S(\boldsymbol{Q}, \omega)$ approximated by the single-phonon term.

As already mentioned, there is a complete lack of calculations of $S(\boldsymbol{Q}, \omega)$ for hcp helium. Also, due to the broad resolution function, separation of these contributions proved impossible. However, some insight can be obtained from the Q-dependence of the observed linewidth (figure 3).

To minimize multi-phonon contributions to $S(\boldsymbol{Q}, \omega)$, measurements were performed at low momentum transfer. Following arguments given by Collins and Glyde [25], the multi-phonon scattering in hcp ^{3}He at our density should be negligible below about 15 nm^{-1}. In this Q-regime, $S(\boldsymbol{Q}, \omega)$ is dominated by single-phonon scattering. No line broadening was detectable at the lowest Q, while, with increasing phonon frequency ω, phonon damping becomes observable. The quality factor $\omega/2\Gamma$ decreases to about 5 at the highest phonon frequencies at the zone centre (001).

The observed linewidth continues to increase over the momentum-transfer range between 12 and 20 nm^{-1}. This suggests that higher-order contributions to $S(\boldsymbol{Q}, \omega)$ gain importance. In particular, the growing broad $S_2(\boldsymbol{Q}, \omega)$ component in the measured spectra might lead to an increase in the fitted width parameter Γ. In this case, analysis of the spectra with the DHO model is not physically meaningful, but can give a description of the unresolved lineshape. Calculations for fcc ^{4}He [25] reveal the importance of the multi-phonon terms in describing the experimental spectra.

Approaching the zone centre (002), the width starts to decrease again. This can be caused by the $(1/\omega)$-dependence of the one-phonon intensity, leading to a relative enhancement of $S_1(\boldsymbol{Q}, \omega)$ compared to $S_2(\boldsymbol{Q}, \omega)$ at low ω. Therefore, the influence of the higher-order terms on the DHO description of the spectra becomes weaker; eventually single-phonon properties dominate.

The ACB sum rule provides a qualitative test for the influence of higher-order contributions to the DHO description of the spectra. According to the ACB sum rule [1, 26]

$$\int_{-\infty}^{\infty} \mathrm{d}\omega\, \omega S_p(\boldsymbol{Q}, \omega) = |G(\boldsymbol{Q}, \boldsymbol{q})|^2 d_{\mathrm{DW}}^2(\boldsymbol{Q}) \tag{6}$$

which is the first moment of the sharp component

$$S_p(\boldsymbol{Q}, \omega) = S_1(\boldsymbol{Q}, \omega) + S_{12}(\boldsymbol{Q}, \omega)$$

of the dynamical structure factor. In hcp ^{3}He along the [001] direction, the square of the inelastic structure factor $\mathrm{G}(\boldsymbol{Q}, \boldsymbol{q})$ reduces to $Q^2/2m$. Thus, if the DHO model is not influenced by any multi-phonon contributions, the first moment calculated from the DHO model, divided by $Q^2/2m$, will follow the Debye–Waller factor. This is shown in figure 7. The deviations from the dashed curve indicate the massive effect of higher-order processes on the observed spectra in the momentum-transfer range from about 15 to 20 nm^{-1}. This is precisely the range of the broadest experimental lineshapes.

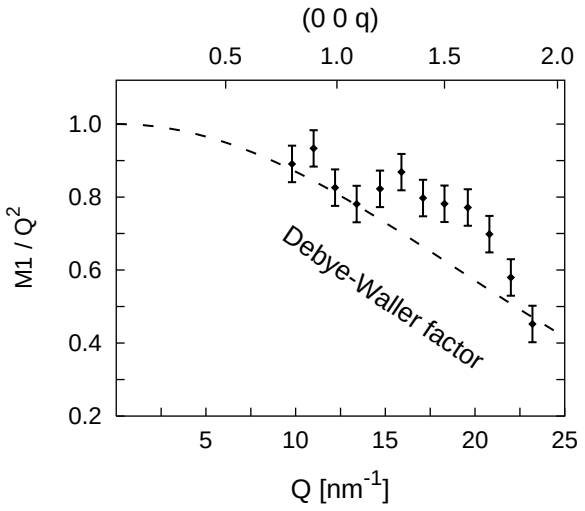

Figure 7. Comparison of the normalized first moment of $S_{\mathrm{fit}}(\boldsymbol{Q}, \omega)$ with the Debye–Waller factor, the first moment of $S_p(\boldsymbol{Q}, \omega)$ according to the ACB sum rule.

6. Conclusions

The first experimentally determined phonon dispersion relation for hcp ^{3}He along the [001] direction was obtained from high-resolution inelastic x-ray scattering. For small momentum transfers, hcp ^{3}He shows well defined excitations, while at high $|\boldsymbol{Q}|$, line broadening becomes the prominent feature of the spectra. This is certainly due to the fact that, in the highly anharmonic system, ^{3}He multi-phonon contributions play an important role. Comparison with the phonon dispersion relation for ^{4}He at the same density indicates a smaller phonon frequency ratio than expected.

Acknowledgments

We wish to thank F Sette, M Krisch, C Masciovecchio, U Bergmann, R Verbeni and B Gorges from ID16 at the ESRF for their valuable technical support during the experiments. We also acknowledge the significant help of M Schreckenberg and U Ponkratz from the Universität Rostock throughout the whole project. The work was supported by BMBF project No 05–650 HRA 1 and by US DOE BES-MS, Contract No DEFG02-96ER45439.

References

[1] Glyde H R 1994 *Excitations in Solid and Liquid Helium* (Oxford: Clarendon) and references therein
[2] Dobbs E R 1994 *Solid Helium Three* (Oxford: Oxford Science)
[3] See, for example,
Scherm R, Guckelberger K, Fåk B, Sköld K, Dianoux A J, Godfrin H and Stirling W G 1987 *Phys. Rev. Lett.* **59** 217
[4] Schell N, Simmons R O and Burkel E 1996 *J. Synchrotron Radiat.* **3** 316
Burkel E, Schwoerer-Böhning M, Seyfert C and Simmons R O 1996 *Physica* B **219+220** 98
[5] Seyfert C, Arms D A, Sinn H, Schreckenberg M, Simmons R O and Burkel E 1997 First observation of phonons in solid ^{3}He *ESRF Annual Report*
[6] Seyfert C, Arms D A, Sinn H, Simmons R O and Burkel E 1996 *Czech. J. Phys.* **46** 471

[7] Burkel E 1991 *Inelastic Scattering of X-rays with Very High Energy Resolution (Springer Tracts in Modern Physics vol 125)* (Berlin: Springer)
[8] Sette F 1995 *ESRF Beamline Handbook* ed R Mason (Grenoble: ESRF) p 99
Sette F, Ruocco G, Krisch M, Bergmann U, Masciovecchio C, Mazzacurati V, Signorelli G and Verbeni R 1995 *Phys. Rev. Lett.* **75** 850
[9] Venkataraman C T and Simmons R O 1996 *Rev. Sci. Instrum.* **67** 3365
[10] Seyfert C 1998 Untersuchung der Gitterdynamik von hcp Helium-3 und Helium-4 mit unelastischer Röntgenstreuung *Dissertation* Universität Rostock
[11] Grilly E R and Mills R L 1957 *Ann. Phys., NY* **8** 1
[12] Fåk B and Dorner B 1992 *ILL Technical Report* No 92FA0085
See also the discussion in reference [1], pp 184–6.
[13] Press W H, Teukolsky S A, Vetterling W T and Flannery B P 1992 *Numerical Recipes in C* 2nd edn (Cambridge: Cambridge University Press) p 689
[14] Ahlers G 1970 *Phys. Rev.* A **2** 1505
[15] Minkiewicz V J, Kitchens T A, Shirane G and Osgood E B 1973 *Phys. Rev.* A **8** 1513
[16] Minkiewicz V J, Kitchens T A, Lipschultz F P, Nathans R and Shirane G 1968 *Phys. Rev.* **174** 267
[17] Reese R A, Sinha S K, Brun T O and Tilford C R 1971 *Phys. Rev.* A **3** 1688
[18] Eckert J, Thomlinson W and Shirane G 1978 *Phys. Rev.* B **18** 3074
[19] Arms D A 1999 *PhD Thesis* University of Illinois, Urbana-Champaign, IL
[20] Gillis N S, Koehler T R and Werthamer N R 1968 *Phys. Rev.* **175** 1110
[21] Morley G L and Kliewer K L 1969 *Phys. Rev.* **180** 245
[22] Chell G G, Goldman V V, Klein M L and Horton G K 1970 *Phys. Rev.* B **2** 560
[23] Sample H H and Swenson C A 1967 *Phys. Rev.* **158** 188
[24] Slusher R E and Surko C M 1976 *Phys. Rev.* B **13** 1086
[25] Collins W M and Glyde H R 1978 *Phys. Rev.* B **18** 1133
[26] Ambegaokar V, Conway J M and Baym G 1965 Inelastic scattering of neutrons by anharmonic crystals *Lattice Dynamics* ed R F Wallis (Oxford: Pergamon) p 261 ff